Particle-Initiated Negative Corona in Co-axial Cylindrical Configuration

M. M. El Bahy*, S. A. Ward**, M. Badawi** and R. Morsi**
*Faculty of Engineering, Benha University, Egypt
**Faculty of Engineering (at Shoubra), Cairo, Egypt

Abstract- **This paper presents theoretical and experimental investigations of the onset voltage of conducting particle-initiated negative corona in air insulated co-axial cylindrical configurations. The conducting particles are spheres or wires of varying dimensions. The particle is fixed either on the inner or outer cylinder. The calculated onset voltage of negative corona is based on the criterion developed for the formation of repetitive negative corona Trichel pulses. This calls at first for an accurate calculation of the electric field in the vicinity of the particle. The investigated gap in the presence of particle is a three-dimensional field problem, due to the asymmetric position of particle inside the gap. The electric field is calculated using the charge simulation technique with a new charge distribution. The effect of varying field nonuniformity, particle shape, size and position on negative corona onset voltage is investigated. Laboratory measurements of negative corona onset voltage as influenced by particle position, shape and dimensions in air insulated co-axial configurations are carried out and compared with the present calculations. The calculated values agreed well with those measured experimentally.**

I. Introduction

The use of gas-insulated systems (GIS) in the power system network has acquired considerable importance because of its compactness, maintenance free, safe and reliable operation. The reliability of GIS is adversely affected by the presence of contaminating conducting particles in the insulation structure. These particles initiate partial discharges forming electrons and ions in the medium, and then initiating the process of breakdown which leads to catastrophic failure of insulation structure [1-6]. These particles drastically reduce the onset voltages of corona and breakdown [2,4,6-8]. Insulating particles are not so harmful as they have little effect on the insulating properties of gases, however 20% of failures in GIS are due to the existence of contaminating conducting particles [9,10]. These particles may have any shape or size. It may be spherical or filamentary (like wire) or in the form of fine dust. Wire like particles are more harmful and their effects are more pronounced at higher gas pressures. The field at the particle tip exceeds the limiting dielectric strength of the gas, at least locally, initiating a corona discharge, which in time develops into a breakdown. The particles may be free to move under the influence of the applied field or may be fixed on the electrodes in the form of a protrusion representing surface roughness. When they are present and are in contact with one of the electrodes, they acquire a charge, depending on the applied field and its size. At a particular field it will lift and move toward the inner cylinder when set free on the outer cylinder. Before reaching the lifting field, the field at the particle may be sufficient to initiate corona discharge.

In this paper, theoretical and experimental investigation of the effect of conducting particle on the onset voltage of negative corona in air insulated co-axial configuration is presented. This configuration has been used for simulating the structure of GIS. Onset voltage of negative corona is investigated since it is somewhat lower than onset values of positive corona [11]. Determination of onset voltage is based on the criterion developed for formation of repetitive negative corona Trichel pulses [12], which requires an accurate calculation of electric field in the vicinity of the particle. The investigated gap in presence of particle is a three-dimensional field problem, due to the asymmetric position of particle inside the gap, where the field is calculated using the charge simulation technique (CST) [6,7,12-14] with a new charge distribution. The conducting particles are spheres or wires of varying dimensions, fixed either on the inner or outer cylinder. The wire particle is a cylinder hemispherically terminated at both ends positioned to touch radially either the inner or outer cylinder. The calculated onset values agree satisfactorily with the values measured experimentally.

II. Experimental Set-up

The experimental work was carried out in laboratory at room temperature (22-25^{o}C) and atmospheric pressure using co-axial cylindrical configuration made of brass. The configurations had inner cylinder of varying radii (5.5, 6, 8 and 11 mm), and outer cylinder of constant radius (41 mm). The inner cylinder length is 800 mm supported at both ends by insulating supports and extended along the axis of 200 mm long outer cylinder. Outer cylinder edge is smoothed and rounded to avoid flashover or early discharge. Different stainless steel spherical particles of radii 0.5, 0.75, 1, 1.25, 1.5 and 2 mm were used. Also, tin wire particles of radii 0.25, 0.375, 0.5 mm and varying lengths in the range 2 to 20 mm were used.

A high-voltage DC source with negative polarity (Hipotronics, Model 800PL-10 MA series) was used to energize the stressed cylinder up to 80kV and the source has a voltmeter for measuring the output applied voltage with an accuracy of ± 2%. The stressed cylinder was connected to the HV source through a water resistance of 1MΩ, as a current limiting resistor, and the other cylinder was grounded through 10kΩ resistor. The waveform of corona pulse was monitored by a digital oscilloscope. The experiments were carried out with a particle fixed either at inner or outer cylinder surface. The voltage drop across the 10KΩ resistor was fed to an oscilloscope.

978-1-4673-1252-3/12/$31.00 ©2012 IEEE

To determine the negative corona onset voltage, the applied voltage was raised step by step until the initiation of the corona pulses on the oscilloscope takes place [12]; the applied voltage is the corona onset value. The time interval between two successive applied voltages was a minimum of 1 min. At least 10 measurements were taken for each measuring point to estimate the average value.

III. Method of Analysis

A. Onset Voltage of Negative Corona

When the electric field strength at the particle tip reaches the onset value for ionization by electron collision, a primary avalanche starts to develop along the direction away from the particle, Fig. 1; where the field assumes maximum values. With the growth of the avalanche, more electrons are developed at its head, more photons are emitted in all directions, and more positive ions are left in the avalanche's wake. The growth of the avalanche continues as long as Townsend's first ionization coefficient, $\alpha(\xi)$, is greater than the electron attachment coefficient, $\eta(\xi)$, and terminates at $\xi=\xi_c$; i.e. at the ionization-zone boundary, ($\alpha(\xi)=\eta(\xi)$) [7], where, the electrons get attached to the gas molecules and form negative ions.

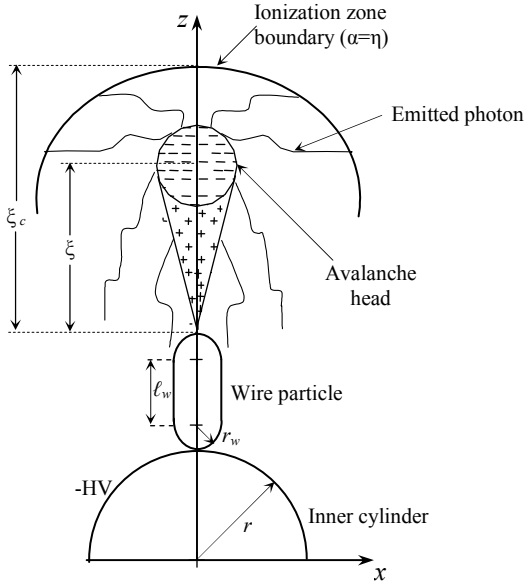

Fig. 1 Growth of the primary avalanche along the gap axis, in negative corona, initiated from tip of wire particle.

For a successor avalanche to be started, the preceding avalanche should somehow provide an initiating electron at the particle tip, possibly by photoemission, positive ion impact, metastable action, or field emission. Field emission is possible only at field strengths exceeding 5×10^7 V/m. Electron emission by positive-ion impact is more than two orders of magnitude less frequent than that by photoemission. Metastables have been reported to have an effect approximately equal to that of positive ion impact. Therefore, only the first mechanism (electron emission from the cathode by photons) was considered in the mathematical formulation of the onset criterion [7], where at least one photoelectron, ($N_{eph}=1$), is emitted by the photons of the primary avalanche to keep the discharge self sustaining [7], i.e.

$$N_{eph} = \gamma_{ph} \int_0^{\xi_c} \alpha(\xi)\ g(\xi)\ \exp\left[\int_0^{\xi_c} (\alpha(\xi)-\eta(\xi))\, d\xi\right] \exp(-\mu\xi)\, d\xi \qquad (1)$$

where, γ_{ph} is Townsend's second coefficient due to the action of photons, μ is the absorption coefficient in air, ξ_c is the distance measured from the particle tip determining the ionization-zone boundary and $g(\xi)$ is a geometric factor to account for the fact that some photons are not received by the cathode [12]. The condition for a new (successor) avalanche to be developed is

$$N_{eph} \geq 1 \qquad (2)$$

The onset voltage of corona does not appear explicitly in relation (1). However, the values of $\alpha(\xi)$, $\eta(\xi)$ which are given in [15] are affected by the electric field produced due to the applied voltage ($-V$). The onset voltage is the critical value, which fulfills the equality (2).

B. Electric Field Calculation on and Around Particle Surface

The analysis is based on CST in which the charge on the surfaces of the particle and the inner cylinder is replaced by a set of fictitious simulation charges arranged inside each of them, wherever, the surface charge on the outer cylinder is replaced by another set of charges arranged outside its surface.

The satisfaction of the pertinent boundary conditions results in a set of equations whose simultaneous solution determines the unknown simulation charges. Knowing the simulating charges, the electric potential and field can be calculated at any point on and around particle surface in the investigated gap [6,12-14].

1) Simulation Technique: The analysis is based on CST [6,12-14] in which the distributed charge on each surface of inner and outer cylinder is replaced by a set of n discrete line charges of varying longitudinal charge density arranged axially inside and outside their surfaces respectively, Fig. 2. Each line charge is divided into definite number k of finite line charges, which is determined according to accuracy level. Hence, the number of simulation charges for each cylinder is $(n\times k)$ charge. The distributed charge on the surface of spherical or wire particle is replaced by 2 point charges and a set of m ring charges arranged inside it, Fig. 2. The ring charges have varying charge density along their entire perimeter. It can be assumed that the ring charge density remains constant within a certain angular range, Fig. 3. Hence, each ring charge is divided in the simulation into definite number of m_1 ring segments with constant charge density (ρ), which is determined according to accuracy level [16].

For the spherical particle, the number of simulation charges inside the particle is $[2+(m\times m_1)]$; i.e. the total number of simulation charges is $N=[(2\times n\times k)+2+(m\times m_1)]$.

The charge over the wire particle is simulated by 2 points, and m rings arranged inside the particle, Fig. 2. For the cylindrical part of the wire particle, the surface charge is simulated by uniformly distributed m_2 rings that vary in number depending on wire shape factor, which is defined as

the wire cylindrical part length (ℓ_w) to its radius (r_w) ratio (ℓ_w/r_w), m_2 equals integer of $[f_1\times(\ell_w/r_w)]$. For each hemispherical tip, the surface charge is simulated by a point charge placed at a distance ($f_2\times r_w$) from the tip center and two ring charges arranged uniformly inside each tip. Each ring is divided in the simulation into definite number of m_1 ring segments with constant charge density (ρ), which is determined according to accuracy level, Fig. 3. Hence, the total number of simulation charges inside the wire particle is $[2+(m\times m_1)]$; $m=(4+m_2)$; i.e. the total number of simulation charges is $N=[(2\times n\times k)+2+(m\times m_1)]$.

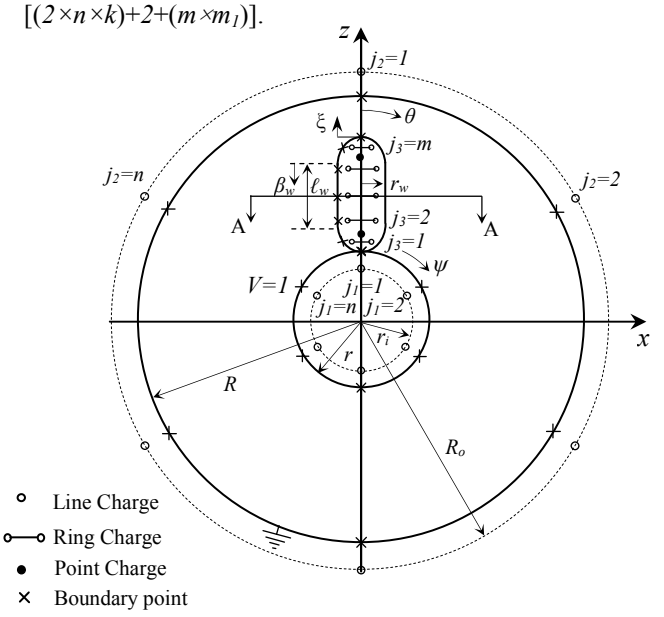

Fig. 2 Discrete simulation charges and boundary points in a cross section of coaxial cylinder gap with a wire particle placed in contact with inner cylinder.

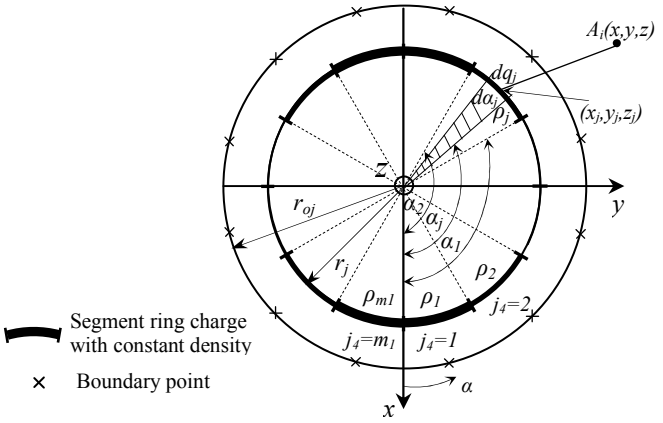

Fig. 3 Discrete simulation ring charge, divided into equal segment ring charges with constant charge density [16], placed at section A-A in Fig.2.

2) Coordinates of Simulating Charges: Fig. 2 shows a cross section of co-axial gap with a wire particle placed in contact with the inner cylinder. Inside this cylinder a simulating n line charges of varying longitudinal charge density are arranged uniformly at a radius of ($f_3\times r$). Outside the outer cylinder, a simulating n line charges are also arranged uniformly at a radius of $R_o=R+(f_4\times r)$. For the spherical particle, the location of the two point charges distant $\pm(f_5\times r_s)$ from the particle centre at z-axis. The first ring charge (i.e. $j_3=1$) is placed at $z_1=r+(f_6\times r_s)$; while the other rings are arranged according to the relation $z_{j3}=[z_1+f_7\times(j_3-1)\times r_s]$, and as shown in Fig. 3, the radius of ring charge is a fraction f_8 of particle radius r_{oj} at the same z-level; $r_{j3}=(f_8\times r_{oj})$.

For the wire particle, a point charge is placed at a distance ($f_2\times r_w$) from the tip center of each hemispherical tip and two ring charges arranged uniformly inside each tip. For the cylindrical part, the surface charge is simulated by uniformly distributed m_2 rings.

The problem is now reduced to the determination of the optimum values of integer's n, k, m, m_1, m_2 and factors f_1 to f_8.

3) Coordinates of Boundary Points: To satisfy the boundary conditions, a boundary point, corresponding to each simulation charge, is chosen along the co-axial cylinders and around the particle surface, Figs. 2, 3. hence, the number of boundary points equals the number of simulation charges *(N)*. The boundary points corresponding to the simulation finite line and segment ring charges were chosen midway along the line and the segment at the cylinders and particle surfaces, respectively. Also, for the simulation point charges, boundary points were chosen at the particle tip and at the touch points.

4) Potential Calculation: The potential (φ_i) at an arbitrary boundary point $A_i(x,y,z)$ is linearly related to all simulation charges by:

$$\phi_i = \sum_{j=1}^{j=N} p_{i,j} q_j \tag{3}$$

where, $p_{i,j}$ is the potential coefficient of the i^{th} boundary point relative to simulation charge q_j. $p_{i,j}$ of point charge is defined in [13,14], $p_{i,j}$ of finite line charge [12,14] is, Fig. 4:

$$p_{i,j} = \frac{1}{4\pi\varepsilon\ell_j}\left[\ln\frac{(\ell_j - y_1)+\gamma}{(-y_1)+\delta}\right] \tag{4}$$

$$\gamma=\sqrt{(x_1)^2+(\ell_j-y_1)^2+(z_1)^2},\quad \delta=\sqrt{(x_1)^2+(y_1)^2+(z_1)^2},$$

$$x_1=(x-x_m),\quad y_1=(y-y_m),\quad z_1=(z-z_m),$$

Where, ℓ_j is finite line charge length, $A(x,y,z)$ and $A(x_1,y_1,z_1)$ is location of boundary point referred to main coordinated system (x,y,z) and new coordinated system (x_1,y_1,z_1), respectively.

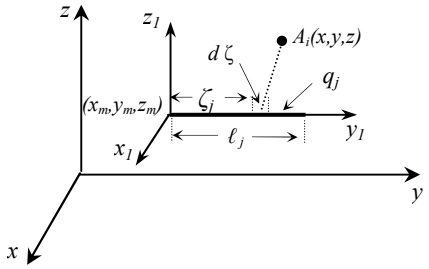

Fig. 4 Finite line charge (q_j) assigned to new coordinates (x_1,y_1,z_1)

For ring segment charge (ρ_j), the potential coefficient $p_{i,j}$ is, Fig. 3, defined in [14]:

$$p_{i,j} = \frac{1}{4\pi\varepsilon(\alpha_2-\alpha_1)}\int_{\alpha_1}^{\alpha_2}\frac{d\alpha_j}{\sqrt{x^2+y^2+r_j^2-2xr_j\cos\alpha_j-2yr_j\sin\alpha_j+(z_j-z)^2}} \tag{5}$$

5) Electric Field Calculation: It is well known that the electric field intensity *(E),* is the negative gradient of the potential. Thus the components of the electric field are:

$$Ex_{i,j} = -\frac{\partial \phi_1}{\partial x}, \quad Ey_{i,j} = -\frac{\partial \phi_1}{\partial y}, \quad Ez_{i,j} = -\frac{\partial \phi_1}{\partial z},$$

Hence, the electric field at an arbitrary point $A_i(x,y,z)$, is the vector sum of the individual components contributed by the point charge [13,14], finite line charge [12,14] and ring segments charge [14].

$$Ex_i = \sum_{j=1}^{j=N} Ex_{i,j}, \quad Ey_i = \sum_{j=1}^{j=N} Ey_{i,j} \quad \text{and} \quad Ez_i = \sum_{j=1}^{j=N} Ez_{i,j} \tag{6}$$

Then, the field intensity at that point is calculated by

$$E_i = \sqrt{Ex_i^{\,2} + Ey_i^{\,2} + Ez_i^{\,2}} \tag{7}$$

IV. Results and Discussions

To check the charge simulation accuracy, check points were chosen midway between the boundary points on the surfaces of the particle and the co-axial cylinders. The potential deviation from the applied voltage and the field deviation from being normal to the surfaces of the particle and the cylinders were assessed to check how well the boundary conditions are satisfied. This check of accuracy was made for (i) a wide range of R to r ratio (1.5 –500), (ii) r_s to r ratio (0.0001– 0.25), (iii) r_w to r ratio (0.005–0.25), the wire shape factor, i.e. the cylindrical part length ℓ_w to wire radius r_w ratio (0.2–78). The accuracy remained the same for these investigated ranges with a maximum percentage voltage error of 0.05% and maximum field deviation angle of 2.5°. Malik [13] has stated that potential error values less than 0.1% are considered reasonable for accurate field solution.

The accuracy of a simulation depends strongly on the assumptions concerned with the choice of the number and the coordinates of the simulation charges. The optimum values of factors f_1 to f_8 are f_1=2, f_2=0.5, f_3=0.1, f_4=5, f_5=0.015, f_6=0.12, f_7=0.045 and f_8= 0.55. The number of charges was found to be: (i) for co-axial cylinders n= 6, k= 100, (ii) for spherical particle m= 12, m_1= 30, (iii) for wire particle m= 4+m_2, m_2= 1-156 for (ℓ_w/r_w)= 1 to 78, m_1= 60. Hence, the total number of simulation charges *(N)* in the presence of spherical particle is 1562 and N in the presence of wire particle varies from 1502 to 10802 for the two limits of the wire shape factor.

A. Simulation Accuracy

When the spherical particle placed at inner cylinder, the maximum potential error does not exceed 1.4×10^{-3}%, while the variation of field deviation from being normal to the spherical particle surface which is placed at inner cylinder is shown in Fig. 5, α, θ start from 0° to 360°, 0° to 105°, respectively. Over most of the particle surface, (except the narrow zone that lies near the touch point as reported before in [12] over the stranded conductor surface), the maximum field deviation from being normal is 2.5°. When the particle is placed at the outer cylinder, the corresponding error values are 1×10^{-3}% and 1.3°, respectively.

Fig. 6, 7 show the variation of field deviation from being normal to the hemispherical tip and the cylindrical part of the wire particle, α, θ start from 0° to 360°, 0° to 90°, respectively, where β_w is the normalized distance from its tip centre, Fig. 2; the maximum field deviation errors are 1.5 and 2.5° respectively. The calculated maximum potential errors don't exceed 0.025%, 1×10^{-4}%, respectively.

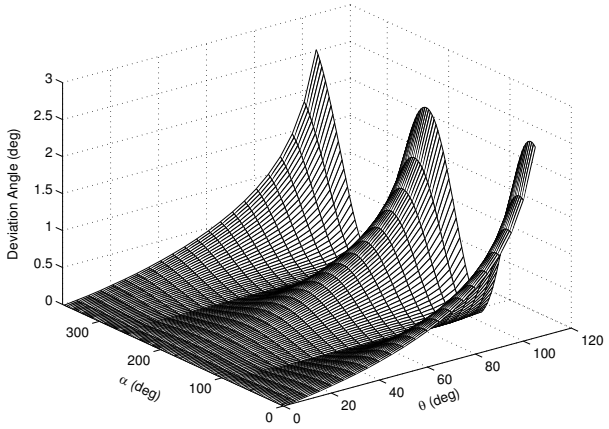

Fig. 5 Variation of deviation angle errors of field around the spherical particle surface lying at inner cylinder, (r_s=1 mm, r=6 mm, R=41 mm).

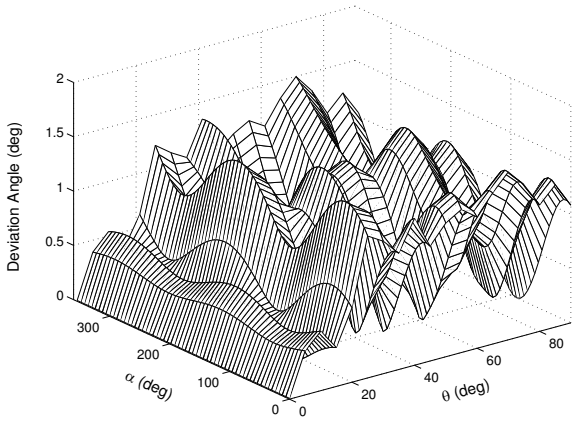

Fig. 6 Variation of deviation angle from being normal to the particle surface around the hemispherical tip of the wire particle (r_w=0.25 mm, l = 5 mm) lying at inner cylinder (r=5.5 mm, R=41 mm), l is total wire length

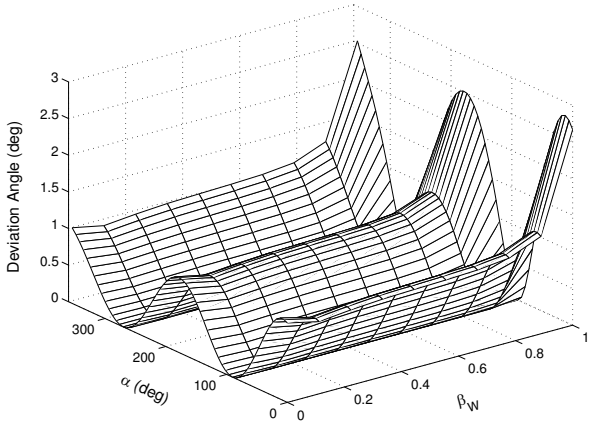

Fig. 7 Variation of deviation angle errors of field around the cylindrical part of the wire particle (r_w=0.25mm, l=5mm) lying at inner cylinder (r=5.5mm, R=41mm).

If the wire particle is placed radially in contact with the outer cylinder, the maximum errors don't exceed 1.5° and 1.2°, respectively, for field deviation from being normal. The calculated maximum potential errors don't exceed 4×10^{-3}% and 1.2×10^{-5}% for the hemispherical tip and the cylindrical part, respectively.

Along the surface of the co-axial cylinders, the percent potential and field deviation from being normal were calculated and were found to be acceptable over a length of 100 times the inner electrode radius *r*.

B. The Field Intensification Factor at Particle Surface Tip

The field intensification factor at the particle surface tip is responsible for the development of corona discharge. For the presence of particle at inner cylinder, this factor is defined as the electric field at the particle tip divided by the field at the inner cylinder of the clean gap.

When the criterion of self-sustained discharge is used to determine the onset voltage of negative corona, the avalanche growth is computed in actual space which depends on the spatial field distribution. To demonstrate the effect of particle shape and size on field intensification factor, Fig. 8 was plotted. In this figure, for shape factors ℓ_w/r_w=20; (ℓ_w=5, r_w=0.25, ℓ_w=10, r_w=0.5), ℓ_w/r_w=10; (ℓ_w=5, r_w=0.5 ℓ_w=2.5, r_w=0.25), the following results are obtained: (a) the field intensification factors are 14.4, 11.2 and 8.6, 10.4, respectively. However, the ionization thickness for these cases is: 0.35, 0.53, 0.54 and 0.367 mm, respectively, i.e. the ionization thicknesses were approximately equal for the wire particles having the same radii and independent of their lengths. However, the corona onset voltages were 8.89, 9.0, 11.98 and 12.55 kV respectively, i.e. the onset voltages are approximately equal for the particles having same shape factors; that's because the onset voltage depends on the growth of the primary avalanche and hence it depends on the spatial field distribution. (b) The figure clearly demonstrates the influence of the wire length on avalanche growth (5/0.25mm, 5/0.5mm, 10/0.5mm). Hence, the thinner one of wire particles having the same length and the longer one having the same radius lead to the onset of corona at lower applied voltages. These concepts agree well with the results obtained in [6]; where the wire particle was found free in uniform field. As shown in figure the spatial field distribution of the bigger spherical particle is higher than the smaller one, hence, the bigger particle will have the smaller onset voltage.

C. A Comparison Between Calculated and Measured Values

Laboratory measurements of the onset voltage of particle-initiated negative corona in air insulated co-axial configuration have been carried out to check the accuracy of present calculation.

Fig. 9 shows the calculated and measured onset voltage of negative corona initiated by spherical particle lying at inner cylinder having different radii in air. As shown in figure, when the particle size increased, a slow reduction in onset voltage is achieved for different inner cylinder radii; because of the difference in spatial field distribution is small; Fig. 8.

Fig. 10, shows the calculated and measured onset voltage of negative corona initiated by wire particle, of different radii and shape factors, fixed radially at inner cylinder surface of air insulated co-axial configuration (r=5.5 mm and R=41 mm).

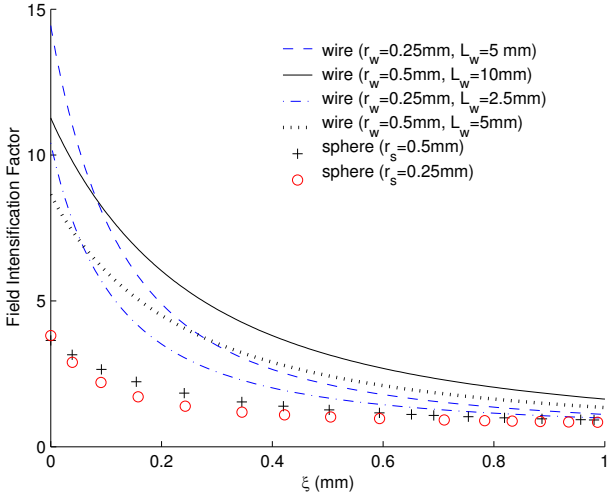

Fig. 8 Field intensification factor of wire and spherical particles lying at inner cylinder (r=5.5 mm, R=41 mm)

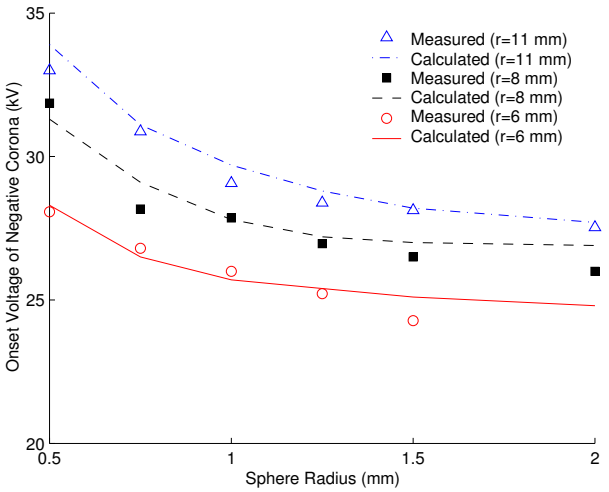

Fig. 9 Measured and calculated onset voltage of corona initiated by spherical particles, lying at inner cylinder of different co-axial configurations, R= 41mm.

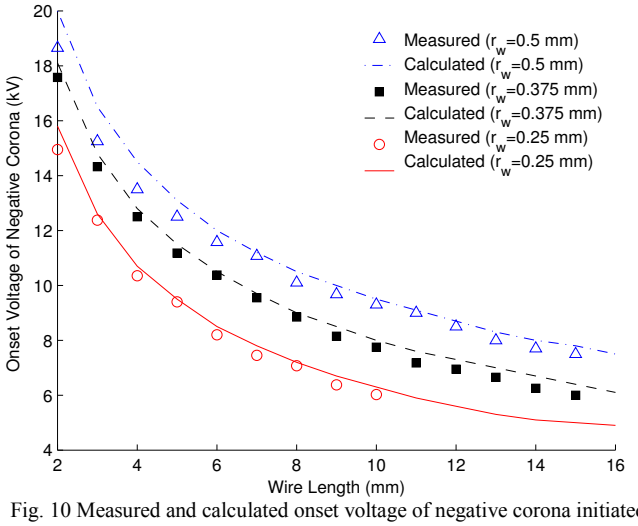

Fig. 10 Measured and calculated onset voltage of negative corona initiated by wire particle of different shape factors fixed radially at inner cylinder.

Fig. 11, shows the calculated and the measured onset voltage of negative corona initiated by wire particle, of different radii and shape factors, fixed radially at outer cylinder surface of air insulated co-axial configuration (r=5.5 mm and R=41 mm).

For the calculated and measured values in Figs. 9, 10 and 11, the maximum percent error between measured and calculated values, in the presence of wire or spherical particles at inner or outer cylinders, is less than 7%. The relative standard deviation of the mean measured values was generally less than 0.5 %.

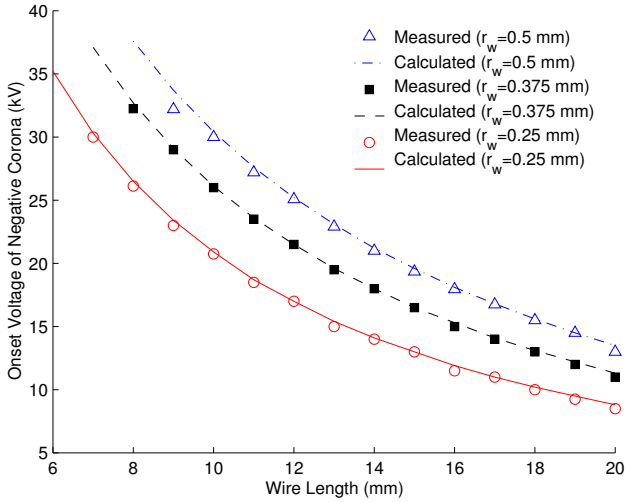

Fig. 11 Measured and calculated onset voltage of negative corona initiated by wire particle of different shape factors, fixed radially at outer cylinder.

Fig. 10, 11 clearly demonstrates the influence of wire length and radius on the onset voltage values for wire particle lying at inner or outer cylinder, where, (a) increasing wire length of same radius (longer one) or decreasing wire radius of same length (thinner one) leads to corona onset at lower applied voltages, (b) the corona onset voltage of wire particles, lying at inner cylinder, having same shape factors is approximately equal. While, the corona onset voltage of wire particles, lying at outer cylinder, having same shape factor is decreased with increasing wire length (longer one), (c) corona onset voltage for wire particle at inner cylinder is less than that for wire particle, of same dimension, at outer one, i.e. presence of wire particle at inner cylinder is more severe than that at outer one.

IV. Conclusions

1. Three-dimensional electric field is accurately calculated in a co-axial configuration in the presence of spherical or wire particles fixed either at inner or outer cylinder using CST.
2. The presence of particle greatly reduces the corona onset voltage and dielectric strength of co-axial configuration, and the presence of particles at inner cylinder is more severe than their presence on the outer one also, the wire particle is more severe than spherical one.
3. The ionization zone thicknesses were approximately equal for wire particles having the same radii and independent of their lengths.
4. For wire particle lying at inner or outer cylinder, increasing wire length of same radius (longer one) or decreasing wire radius of same length (thinner one) leads to onset corona at lower applied voltages.
5. The corona onset voltage of wire particles, lying at inner cylinder, having the same shape factors is approximately equal. While, the corona onset voltage of wire particles, lying at outer cylinder, having the same shape factor is decreased with increasing wire length.
6. The spatial field distribution of the bigger spherical particle is higher than the smaller one, hence, the bigger particle will have the smaller onset voltage.
7. The maximum percent error between measured and calculated onset voltages in the presence of wire or spherical particles at inner or outer cylinders does not exceed 7 %.

References

[1] Cigre working group D1-11, "Knowledge rules of partial discharge diagnosis in service," Electra 207, pp. 63-66, 2003.

[2] I.A. Metwally, A.A. A. Rahim, "Factors affecting the dynamics of wire particles in gas insulated systems," European Transaction on Electric Power, vol. 11, no. 6, pp. 403-412, 2001.

[3] R. Sarathi, R. Umamaheswari, "Understanding the partial discharge activity initiated by a conducting particle in GIS under DC voltages using UHF technique," Journal of Electrical Engineering, vol. 60, no. 3, pp. 136-142, 2009.

[4] C. M. Cooke, "Ionization, electrode surface and discharge in SF_6 at extra-high voltages," IEEE Trans. on PAS, vol. 94, no. 5, pp. 1518-1523, 1975.

[5] F. A. M. Rizk, C. Masetti, R. P. Comsa, "Particle-initiated breakdown in SF6 insulated systems under high direct voltage," IEEE Trans. on PAS, vol. 98, no. 3, pp. 825-836, 1979.

[6] H. Anis and K. D. Srivastava, "Free conducting particles in compressed gas insulation," IEEE Trans. on EI, vol. 16, no. 4, pp. 327-338, 1981.

[7] M. Abdel-Salam, A. Ahmed, and A. Nasr EL-Deen, "Inception voltage of corona discharge from suspended, grounded and stressed particles in uniform-field gas-insulated-gaps at varying pressures," International Journal of Plasma Environmental Science and Technology, vol. 4, no. 1, pp. 1-12, March 2010.

[8] I.A. Metwally, A. A. A. Rahim, "Dynamic analysis of spherical metallic particles in non-uniform electric field," IEEE Transactions on Dielectrics and Electrical Insulation, vol. 9, no.2, pp. 282-293, 2002.

[9] K. B. Madhu Sahu and J. Amarnath, "Effect of various parameters on the movement of metallic particles in a single phase gas insulated bus duct with image charges and dielectric coated electrodes," ARPN Journal of Engineering and Applied Sciences, vol. 5, no. 6, pp. 52-60, June 2010.

[10] K. B. V. S. R. Subrahmanyam and J. Amarnath, "Image charge effect on metallic particle in single phase gas insulated bus duct (GIB)," Journal of Emerging Trends in Engineering and Applied Sciences, (JETEAS), vol. 2, no.3, pp. 451-455, 2011.

[11] Kazutoshi Asano, Kyoko Yatsuzuka and Tomoko Yamaki, "DC Corona Discharge of a Metal filament Particle Within Parallel-Plate Electrodes," IEEE Trans. on Industry Application, vol. 36, no. 1, pp. 87-92, 2000.

[12] M. M. El-Bahy, M. Abouelsaad, N. Abdel-Gawad and M. Badawi, "Onset voltage of negative corona on stranded conductors," Journal of Physics D: Applied Physics, vol. 40, no. 10, pp. 3094-3101, 2007.

[13] N. H. Malik, "A review of the charge simulation method and its applications," IEEE Trans. on Electrical Insulation, vol. 24, no.1, pp. 3-14, 1989.

[14] D. Utmischi, "Charge substitution method for three-dimensional high voltage fields," Third International Symposium on High Voltage Engineering, 28-31 August 1979, Milan, paper 11.02.

[15] Tiebing Lu, Gaolin Xiong, Xiang Gui, Hong Rao and Qi Wang, "Analysis of corona onset electric field considering the effect of space charges", IEEE Trans. on Magnetics, vol. 47, no. 5, pp. 1390-2393, May 2011.

[16] M. M. El Bahy, S. A. Ward, R. Morsi and M. Badawi, "Particle-initiated breakdown in gas-insulated co-axial configuration," Conference on Electrical Insulation and Dielectric Phenomena, 16-19 October 2011, Cancun, Mexico, pp. 722-727.